Materials and Design 187 (2020) 108377

Contents lists available at ScienceDirect

Materials and Design

journal homepage: www.elsevier.com/locate/matdes

Multi-purpose structured catalysts designed and manufactured by 3D printing

Anna Lind, Ørnulv Vistad, Martin Fleissner Sunding, Kari Anne Andreassen, Jasmina Hafizovic Cavka, Carlos A. Grande *

SINTEF Industry, P.O. Box 124 Blindern, NO-0314 Oslo, Norway

HIGHLIGHTS

- A method to control macro and micro porosity of catalysts is presented.
- Porosity of the catalyst can be designed by mathematical functions and then realized by 3D printing.
- A hybrid catalyst with anodized alumina on an aluminum body was manufactured and scaled up.
- The catalyst was tested for NO oxidation to NO2 in a very corrosive media.

GRAPHICAL ABSTRACT

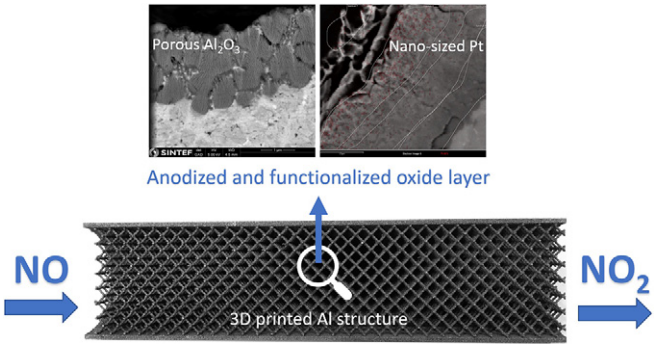

ARTICLE INFO

Article history:
Received 26 September 2019
Received in revised form 1 November 2019
Accepted 19 November 2019
Available online 22 November 2019

Keywords:
3D printing
Catalyst
Anodization
Process intensification
Diffusion
Heat transfer

ABSTRACT

This work presents an example of the design and manufacture capabilities that 3D printing can introduce in catalysis. A multi-purpose catalyst, with fast heat and mass transfer and low-pressure drop has been designed and manufactured by 3D printing. The novelty of the methodology is the combination of advanced techniques for accurate control on the micropore-level allied with a generic framework for the design of macropore and structural levels. The ability to design ordered macroporous should be combined with adequate and controllable implantation of surface functionalities. With this combination of advanced techniques for macro and micro-pore control, it is possible to produce catalysts that unlock traditional trade-off compromises between diffusion, pressure drop and heat transfer.

To demonstrate this novel methodology, we have designed and 3D printed a cubic iso-reticular foam in AlSi10Mg. After producing the support, its entire internal area was anodized to high-surface alumina followed by Pt deposition. We have verified the reproducibility of this technique by manufacturing a catalyst for a demonstrator with 8 m length. The test reaction was oxidation of NO to NO_2 with the main aim to accelerate this reaction for additional recovery of energy in the production of nitric acid.

1. Introduction

Around 90% of all the chemical processes currently in use have a catalytic step [1], and 80% of these are based on heterogeneous catalysts

* Corresponding author.
E-mail address: carlos.grande@sintef.no (C.A. Grande).

https://doi.org/10.1016/j.matdes.2019.108377

[2]. Despite the diverse research program targeting catalyst development, most heterogonous catalysts are still based on spherical granules or extruded pellets. Foams and honeycomb monoliths have niche applications.

Additive manufacturing (AM) or 3D printing (3DP) techniques have been known for more than 30 years but it is only recently that this fabrication method started to be investigated for the design and production of novel catalysts [3–12]. Most of these initial publications focus on the properties of the 3D printed materials and describe the benefits of mixing due to intercalated shape patterns. However, the great and yet unexplored benefit of using 3DP for catalyst design is that the structure can be computer designed to satisfy multiple or multi-task criteria. Manufacturing tailored shapes can allow new operating windows for catalytic processes, modifying the classical trade-off limitations of operation. The catalyst shapes can then be optimized to improve flow patterns but also to maximize heat and mass transfer. The works with catalysts produced by 3DP focused on ceramic or polymer materials so tackling enhanced heat transfer was not considered in previous literature.

Alternatives for accelerating heat transfer to or from the reaction media are the utilization of coated metals [13–15] or supports made of highly conductive materials like silicon carbide [16,17]. Coating a catalyst that can deliver fast heat transfer can result in spalling and detaching of the catalytic layer due to stress-induced fatigue [18]. Moreover, if the structure of the support is intricated, several measures should be taken to ensure uniformity [19,20]. For introducing washcoats, the viscosity, pH, particle size and loading will influence the coating uniformity but may also introduce constraints in the adhesion and metals that can be applied in situ [21].

3DP has been successfully used for manufacturing diverse types of objects in architecture [22,23], parts for industry [24], bone implants [25], etc. Catalysts can be produced with many different materials, but for harder conditions found in many chemical reactions (temperature, pressure, pH), metal and ceramic materials are relevant. The combination of a ceramic porous material and a metallic structure can deliver enhanced properties that benefit mass transfer (porosity of the ceramic) and heat transfer (fast conduction through the metal).

This publication presents a methodology for the design and manufacture of a catalyst with controlled macropore and micropore structures. The catalyst is a 3D printed iso-reticular aluminum foam with anodized surface to generate local porosity to accommodate Pt as the active metal. AM has been an enabling technology once that the shape produced in this work cannot be produced by any other means. Using electrolysis to generate alumina in-situ allows tuning of the microporosity by changing electrolysis conditions [26]. This alumina outer porosity ensures that diffusional resistances are reduced. Furthermore, the open macropore 3D printed structure results in low pressure drop and enhanced flow mixing. Since the catalyst structure is made from metal, it can transport heat faster (to or from the reactor). The in-situ generation of alumina ensures a small and uniform layer over intricated structures while at the same time minimizing thermal stresses.

As an example of the capabilities of this design approach, we have used this catalyst for the bulk oxidation of NO to NO_2 in the presence of water under industrial conditions for the production of nitric acid. The reaction is extremely corrosive [27], equilibrium limited, and has a heat of reaction of −114 kJ/mol.

2. Catalyst design methodology

2.1. Generation of catalyst macro-structure

Open-cell foams are porous supports that allow good radial mixing. Having enhanced radial mixing contributes to transport heat faster to or from the surroundings. Although a thorough work has been done in controlling the foam structure to a good extent, small size distributions still exist in commercial foams. For some very exothermic reactions (or successive reactions), even small variations in the catalyst structure, the heat distribution and dissipation can result in a loss in selectivity and potentially undesired temperature fluctuations [28–30].

The novel design methodology is based on dividing the desired volume of the foam into an array of space-filling solids to produce a tilling without voids. In this tilling, each space-filling solid will constitute one cell. If all cells are of equal dimensions, we set up the basis for the generation of an iso-reticular foam. To make each cell, it is necessary to subtract to the original space-filling solid, a similar solid with smaller dimensions (centered at the same point), and the walls, to provide interconnectivity between the cells. A given number of desired walls (n) of each cell are removed by m-sided prisms being m the number of edges of the cell side. Replicating this operation over all cells in the desired foam dimensions, is possible obtain an open-cell iso-reticular foam by design.

The main advantage of this methodology is that the strut dimensions and the foam porosity can be kept as independent variables. In order to change the porosity without changing the strut dimension, another space-filling solid should be selected. Moreover, to further promote mixing, it is possible to rotate the cells with respect to the inlet of fluid. It has been reported that for lower velocities, the pressure drop is a function of the rotation angle [31], while for very turbulent flows, the cell shape and the porosity are the main parameters [32]. Cell rotation with respect to the flow direction has also proven to be beneficial to reduce the height of theoretical plates in chromatography [33].

2.2. Generation of catalyst micro-structure

When the reaction rate is very fast, diffusional resistances can dominate the entire reactor performance. One strategy to deal with such diffusion-limited problems is to use a catalytic layer only in the external part of the catalyst structure, resulting in a so-called “egg-shell” catalyst. Coating is the most used technique for deposition of a catalytic layer in a structured catalyst. Three-way catalysts are the most popular example where the catalyst is coated to a cordierite (ceramic) substrate. When a ceramic material is coated on a metallic substrate, the very different thermal expansion coefficients can result in spalling if the process has frequent stops or large thermal oscillations.

In this work we have adopted an alternative approach which consists in the electrolytic anodization of the external layers of aluminum into alumina. Anodization of aluminum (Al) and Al alloys has been studied for decades and has applications in multiple areas [26,34,35]. In catalysis, anodization is normally conducted on aluminum foil creating a stable Al_2O_3 layer with a perfectly ordered array of pores [36–39]. The surface area of the catalyst can then be functionalized by deposition of noble or transition metals [40–42]. It has been shown that the pore ordering, pore size, and thickness of the alumina layer can be controlled by varying anodization conditions such as pH and type of electrolyte [43–45], potential [46–48], current [49,50] and temperature [51] on pure aluminum or aluminum with small contaminant content (6060 or 6061 alloys). Sulfuric acid gives the smallest pores, oxalic acid gives an intermediate pore size and phosphoric acid the largest pore size [52–55]. A novelty of the present study is to form a nano-porous oxide layer on the internal surface of the 3D printed cubic iso-reticular foam.

3. Experimental methods

3.1. Support preparation

The catalyst macro-structure used in this work is a cubic-cell iso-reticular foam with a rotation of 45° in one coordinate. The design, manufacturing and characterization of these structures has been described in detail in a previous work [32]. We have proven that the differences between designed and achieved porosity is very small. The supports were printed in PRODINTEC (Spain) using the direct metal laser sintering (DMLS) technique. The equipment used is an

EOS M280 (Germany) and the material is the EOS commercial aluminum alloy AlSi10Mg. To have the possibility of self-supporting and to further promote fast heat transfer from the tubular reactor, the metal iso-reticular foam was designed with an external wall that was also printed. Fig. 1 shows a cross-section over the length of the printed structure. The "as 3D printed" dimension of the macrostructures are 2.1 cm diameter and 20.0 cm length. Different experiments were made on cut-outs of the samples with different lengths (keeping the diameter): 1, 10 and 20 cm.

3.2. Anodization procedure

Before anodization, the aluminum surface was pretreated in two steps. First, the aluminum structure was degreased by sonication in acetone for 15 min at room temperature. Then, the dried structure was soaked in 1 M sodium hydroxide (Merck) for 2 min at room temperature before rinsing with deionized water to remove contaminants and to smoothen the surface. During the anodization, the pretreated aluminum structure was the anode and a solution of 10–15% of sulfuric acid (puriss, 95–97%, Sigma-Aldrich) was used as the electrolyte. A platinum coil (0.5 mm Pt wire, K.A. Rasmussen, Norway) was used as cathode. An illustration of the electrochemical setup is included in the supporting information (Fig. S1). A fixed potential was applied to the system during the anodization process and the current was changing during the reaction going through a maximum before reaching an equilibrium. The variation in electrical current was recorded for the entire duration of the experiments. A typical curve showing the variation of current density with time is presented in the supporting information (Fig. S2).

There are two main challenges in anodizing the internal structure of the 3D printed cellular structure. The first challenge is related to the material. The most employed aluminum alloy for 3D printing, AlSi10Mg alloy, has a high (10%) silicon content. Anodizing this alloy is significantly different from anodizing pure aluminum or aluminum with small amounts of other elements (like 6060 or 6061 alloys). During the anodization of the AlSi10Mg alloy, there will be an enrichment of Si in the oxide layer. Enrichment of the alloying elements in the anodic oxide film is a known phenomenon described in the literature [56–62]. The second challenge is related to the anodization of complex shapes. Two factors can result in a non-homogeneous layer of alumina in the foam:

(1) the rough inner surface of the structure is not directly accessible (as in the case of fully exposed thin films),
(2) the gas bubbles resulting from the oxidation of Al to Al_2O_3 will be trapped inside the foam.

Improved operating conditions to obtain an acceptable alumina support were obtained after a systematic study of the anodization parameters. An additional target was to minimize (suppress if possible) the formation of SiO_2 during anodization. We studied the following anodization conditions: concentration of electrolyte, potential, anodization time and length of the structure to be anodized. The interval of the variables studied in the anodization process is summarized in Table 1. The effect of each of these variables is provided in the supporting information. It has been reported in the literature that sulfuric acid is one of the most suitable for high Si aluminum alloys [63], and therefor this acid was chosen as electrolyte.

3.3. Catalyst impregnation

Deposition of platinum in the porous oxide layer obtained by anodization was performed by wet impregnation [64,65]. Only the inner surface of the cylindrical structures was exposed to the Pt source. As platinum source we have used a commercially available diamminedinitritoplatinum(II) solution: $Pt(NH_3)_2(NO_2)_2$, 3.4% Pt in dilute ammonium hydroxide from Sigma Aldrich. Before impregnation, the supports were cleaned with pressurized air to remove possible residues from the anodization process and then dried at 150 °C. All the samples were exposed to the Pt solution for 2 min. After this exposure time, the excess solution that was not adsorbed inside the porous alumina layer was removed by vigorous shaking. Afterwards, the samples were dried in air at 80 °C overnight. The calcination of the catalysts was carried out at 300 °C for 6 h and with a heating rate of 3 °C min^{-1} passing a flow of helium (flow rate = 60–80 cm^3 min^{-1}) through the samples [66]. Before the testing and before using them in the industrial demonstrator, the samples were further reduced with hydrogen (99.999% purity, Yara, Norway) at 300 °C for 3 h.

3.4. Characterization methods

The microstructure and composition of the anodized samples were analysed using scanning electron microscopy (SEM, Nova NanoSEM650 from FEI Corp) and energy dispersive spectroscopy (EDS, X-Max 50 System from Oxford instruments). Compositions were determined using the Aztec software (Oxford instruments) and were based on calculated standards. Both the surface and polished cross-sections of the anodized 3D printed parts were characterized.

Surface area was determined from nitrogen adsorption at 77 K by a Monosorb instrument (Quantachrome, USA) with a measurement range of 0.01–3000 m^2/g and typical 0.5% reproducibility. Samples were activated under vacuum at 150 °C overnight prior to the measurements.

3.5. Reaction testing

NO oxidation experiments were conducted in a set-up unit already described [27] but instead of the reactor being differential, a Pt-impregnated 3D printed iso-reticular foam with 2 cm length and 2.1 cm diameter was used. A picture of catalyst in the reactor is shown in the Supporting Information. Experiments with 5% of NO were made in the presence of 20% of water at a pressure of 4.7 bar and 300 °C. These are similar conditions as the ones found in modern dual-pressure nitric acid

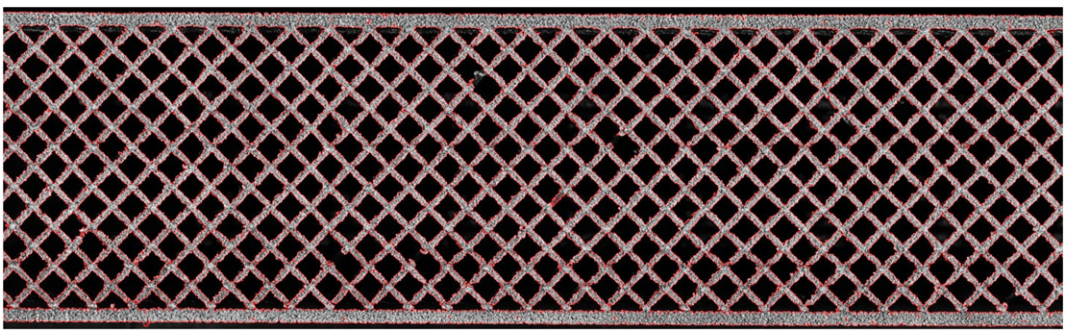

Fig. 1. Longitudinal cross-section of the 3D printed open-cell foam used as the catalyst macro-structure. Length: 10 cm; diameter: 2.1 cm.

Table 1
Summary of variables in the anodization process.

Variable	Range
Sulfuric acid concentration	10–15%
Potential	10–22 V
Anodization time	0.5–120 min
Equilibrium current density	1.5–3.5 A/dm^2

plants. These experiments are very corrosive, and they should be performed with extreme caution.

4. Results and discussion

Performing the anodization of the 3D printed parts with higher voltage, higher electrolyte concentration and/or longer time, will give an increased Si enrichment. On the other side, softer anodization conditions (lower voltage, lower electrolyte concentration and short anodization times) will render lower porosity and a very thin oxide layer. With a parametric study of the anodization process (described in more detail in the supporting information) we have observed that it is possible to decrease the SiO_2 content in the external oxide layer from as high as 80 wt% down to approximately 10 wt% by changing the anodization parameters. Based on this parametric study, the selected anodization conditions were: electrolyte concentration of 15% H_2SO_4 in water and voltage of 15 V.

The length of the 3D printed structures is also crucial for the anodization. Since the studied foam is covered by an external solid wall, the concentration of electrolyte inside the structure might locally change, particularly in the case of longer structures. Moreover, in larger structures the gas bubbles generated from the anodization process will take longer to be evacuated from the structures, reducing locally the surface contact with the electrolyte. In scaling-up anodization conditions, attention should be paid to the overall surface area of the material. Different areas will affect the overall resistance of the system, which had to be taken into account when scaling up the electrochemical setup and also the size of the cathode to avoid overheating.

We have studied the anodization of structures with the same diameter (~21 mm) and different lengths; 1, 10 and 20 cm. Scanning electron microscopy (SEM, *Nova NanoSEM650* from *FEI corp.*) and energy dispersive spectroscopy (EDS, *X-Max 50* system from *Oxford instruments*) data were recorded in pre-specified positions of the anodized structures in order to have a mapping of the size and the composition of the oxide layer. The structure with 1 cm length was short enough to have a good contact with the electrolyte in all the sample, and the anodization process posed no problems to obtain a homogeneous layer in the whole part. Also, for the structure with 10 cm length it was possible to optimize the setup and produce a homogeneous oxide layer throughout the structure. The anodization should be performed using 15 V for a period of 15 min with a solution of 15% of sulfuric acid in water as electrolyte.

For the structure with 20 cm length it was not possible to find anodization conditions giving a homogeneous oxide layer throughout the structure (see Fig. S5). In all the tested conditions, when using 20 cm structures, the alumina layer in the center was thinner than in the extremities.

Therefore, the size of the structures where platinum was deposited was 10 cm length. This procedure was repeated for 80 parts. Fig. 2 shows SEM images of one of the aluminum structures. EDS of this sample shows about 30% SiO_2 in the oxide layer. Fig. 2a shows the morphology of the anodized struts inside the structure. It is expected that with the overall rugosity of the sample, the results will be very different than the perfect honeycomb arrays reported in thin and straight aluminum films. Fig. 2b–d show detailed views of a cross-section of the oxide layer. Fig. 2b shows the grain structure where the anodized alumina on the surface is darker. Fig. 2c shows a further magnification where is possible to see that the alumina oxide is ordered at the grain level. In Fig. 2d the Si rich areas are colored red for clarity. It can be seen that some of the Si is also diffusing to the surface which explains the 30% of SiO_2 compared to the 10% of silicon in the alloy. Similar pictures were recorded for some of the 80 samples prepared with good reproducibility.

Fig. 3 shows SEM results where measurements of the thickness of the alumina layer were recorded in different positions. Several measurements confirmed that the thickness of the oxide layer is between 3 and 4 μm in different parts of the structure. These samples have a SiO_2 content of approximately 30–35% in the oxide layer. The larger amount of SiO_2 in the surface is caused partially by some migration of Si to the surface but also due to some dissolution of the alumina in the external layer. In the case of this alloy, some alumina grains are "peeling off" during the anodization process leaving the structure of SiO_2 that can be seen also in Fig. 3. We did not account the SiO_2 layer to estimate the size of the Al_2O_3 oxide layer.

The generation of alumina on the surface of the 3D printed iso-reticular foam structures results in a net increase of the surface area. BET measurements show an increase in the surface area from 0.1 m^2/g (foam) for an untreated aluminum sample to 1.5 m^2/g(foam) for an anodized sample. The small value of surface area is due to the large mass of the aluminum body. The surface area of the porous alumina (assuming that alumina density is 4.0 g/cm^3 and silica is 2.65 g/cm^3), is estimated to be ~50 $m^2/g(Al_2O_3)$.

One of the benefits of the direct anodization process is that the oxide layer is chemically attached to the metal body. This should render a much higher mechanical resistance in case of thermal oscillations. In cases where the temperature of the process is approx. 300–350 °C and with possibility of frequent stopovers, it is desired that the catalyst is stable. To test the resistance of the produced 3D printed anodized foam, one sample was heated to 350 °C over night and then cooled down before it was hit mechanically. Fig. 4 shows SEM images before and after the heat and "mechanical" treatment. The results show that the sample can withstand some thermal and mechanical treatment, which indicates that the anodization procedure produces an alumina layer that is stable for demanding operating conditions. However, more tests should be done to determine the overall resistance, particularly to thermal oscillations.

The distribution of the platinum introduced by wet impregnation was examined by SEM. Fig. 5 shows SEM images of both the surface (Fig. 5a) and the cross-section (Fig. 5b). The results indicate that platinum is quite evenly distributed, both over the surface and through the porous layer. The size of the Pt particles/clusters was estimated to be in the range 20–50 nm.

The individual cells of the 3D printed iso-reticular foam were designed with a strut half-thickness of 0.15 mm for a 2 mm overall cell length. An observed oxide thickness of 3 μm in all the available area of the struts imply that the fraction of alumina is ~2% of the foam. The value calculated from the BET measurements, indicate that this value is approx. 3 wt%. This can be explained by the difference between the real surface area (including the rugosity as observed in Fig. 2) and the design surface area. The total amount of platinum on the sample is 0.12 wt% determined by weight measurements during the sample preparation. This corresponds to an average of 4.1 wt% Pt in the alumina layer.

This catalyst was developed to perform the oxidation of NO to NO_2 for the synthesis of nitric acid. The NO oxidation is an homogeneous reaction normally regarded as a fast reaction. However, in the industrial production of fertilizers, the rate of heat exchange is faster than the rate of conversion [27]. The conversion of NO in industrial plants at 300 °C is approximately 24%, which is far away from the equilibrium conditions (~95%). If the rate of NO oxidation is increased by a catalyst, additional energy can be recovered in existing units contributing to a process intensification strategy that can be retrofitted to existing plants.

Since the gas velocity is very high (~20 m/s), the iso-reticular foam was designed to have a higher porosity which will render a lower

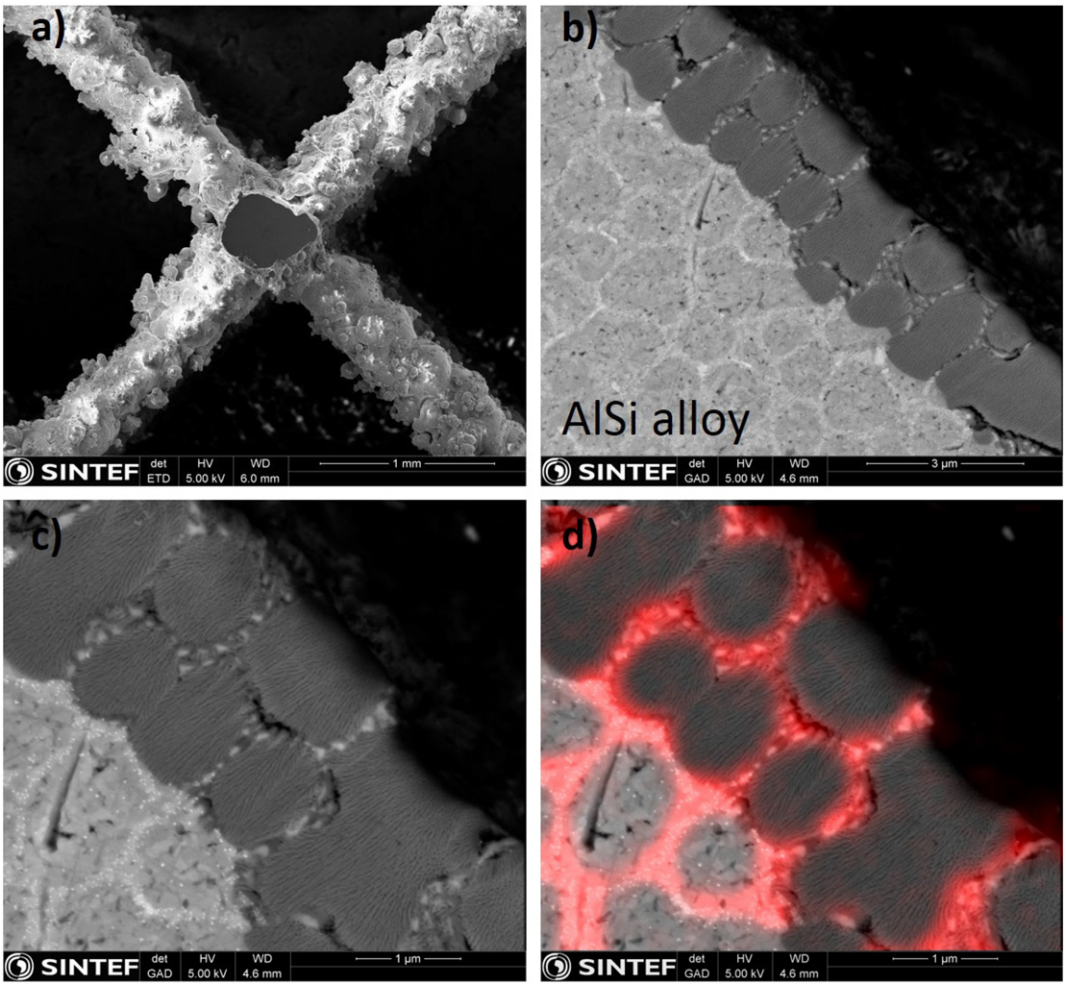

Fig. 2. SEM images of a structure with 1 cm length anodized with 15 V for 15 min in a solution of 15% sulfuric acid, where a) shows the anodized struts inside the structure, b–d) are the cross-section of one oxide layer. In d) the superposition of the SEM picture and the EDS mapping is shown which enhances visualization of Si rich areas.

pressure drop. Moreover, the egg-shell catalyst should contribute to minimize diffusional effects. Keeping the catalytic layer in direct contact with an aluminum body should also enhance the heat transfer to the surroundings in this exothermic reaction.

Experiments were performed for different amounts of oxygen in two different samples of the produced foam. The oxidation results are shown in Fig. 6 for two different samples to demonstrate the reproducibility of the method. The temperature at the exit of the reactor is increased by less than 1 K after the reaction started. This is expected because of the high heat transfer coefficient of the foams (U ~ 1000 W/m^2/K) [32]. The conversion with 8% of oxygen in the gas phase (conditions at the plant) is approx. 50% in a very small piece of catalyst, demonstrating

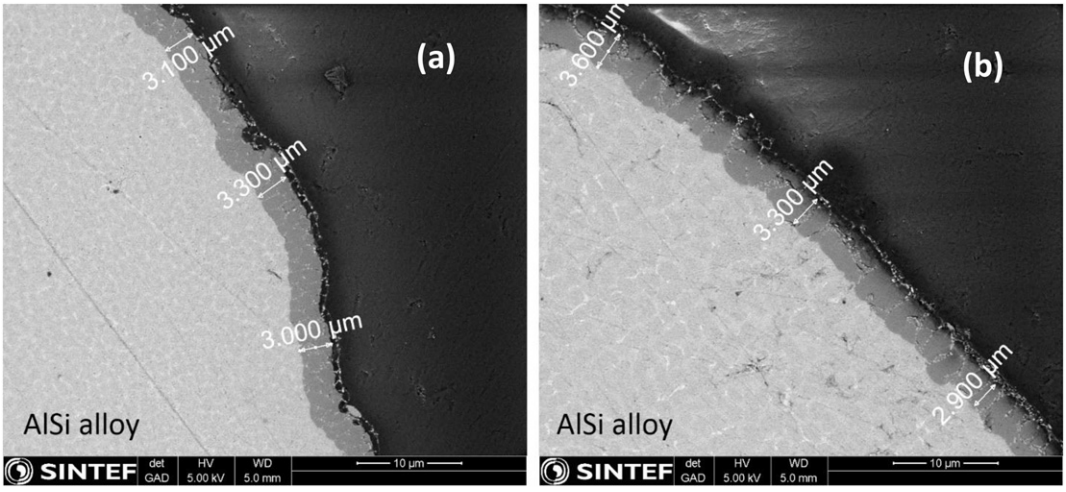

Fig. 3. SEM images of a structure with 10 cm length anodized using 15 V for 15 min in a solution with 15% sulfuric acid in water as electrolyte. The thickness of the oxide layer is the same close to the edges of the structure (a) as in the center of the structure (b).

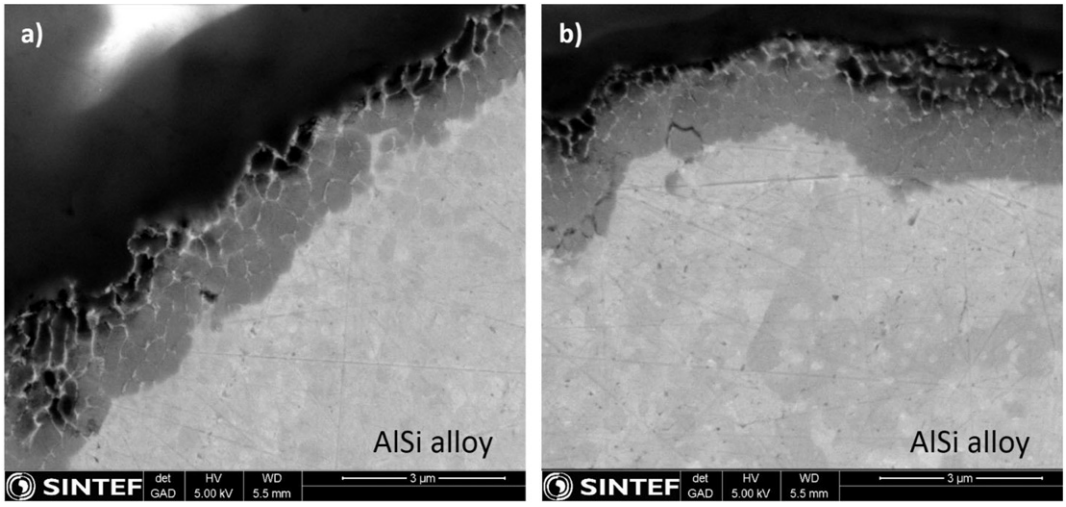

Fig. 4. SEM images of a structure with 10 cm length anodized using 15 V for 15 min in a solution with 15% sulfuric acid in water as electrolyte before (a) and after (b) heat and mechanical treatment at 350 °C.

that this catalyst can be used for process intensification of existing nitric acid plants. Moreover, the good reproducibility of the experimental data indicates that the generation of macro and micro-porosity is reproducible and homogeneous. Once that the methodology to produce homogeneous catalysts was validated, we have produced 80 foam catalysts (of 10 cm length and 2.1 cm diameter) of such catalysts in order to fill a demonstrator unit with a length of 8 m.

5. Conclusions

This work presents a new methodology for catalyst design and manufacture allowing full control of catalyst structure. The main advantage of this methodology is the preparation of structured catalysts with hybrid properties. Hybrid properties can be obtained by a targeted design of macro-structures to facilitate heat transfer and by selective treatment of the produced surface to increase conversion. Indeed, using 3D printing techniques, a scalable structured catalyst can be designed and manufactured to the cell and strut level. Additionally, using lattices with different geometrical shapes is possible to expand the classical limitations and trade-offs between mass, energy and momentum transfer.

In this work we have also demonstrated that is possible to generate a layer of anodized alumina with homogeneous thickness in an intricated Al support produced by 3D printing. Such layer can reduce spalling problems since is chemically linked to the support. This hybrid structure has multiple advantages for reactions that are fast and very exothermic (or endothermic); the thin layer of alumina will minimize diffusion limitations resembling an egg-shell catalyst and the fast and local contact between the catalytic layer and a metallic body helps in fast heat removal.

The anodized cubic iso-reticular foam was used for impregnation of Pt as a catalyst for the oxidation of NO to NO_2. We have seen a much faster heat transfer when compared with an empty tube or with a classical alumina catalyst. Moreover, the conversion of NO to NO_2 was around 50% using a small catalyst, which is much higher than the existing 24%.

This work shows one of the possibilities of using 3D printing as a tool for preparation of hybrid catalysts. Using 3D printing as manufacturing technique for catalysts can result in increased versatility leading to shapes that cannot be achieved with traditional manufacturing. Such materials can be particularly useful in reactions where diffusion, mixing and/or heat transfer limit the performance.

CRediT authorship contribution statement

Anna Lind: Funding acquisition, Conceptualization, Investigation, Data curation, Writing - original draft. **Ørnulv Vistad:** Funding

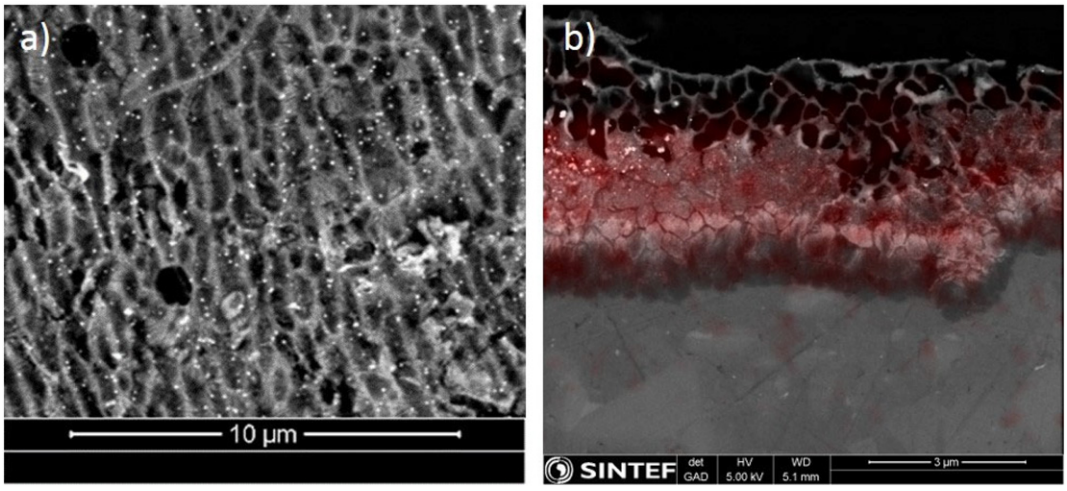

Fig. 5. SEM images showing the platinum distribution a) view from the top to a section of the surface (as white dots) and b) cross-section of one strut where SEM and the Pt-EDS map are superimposed.

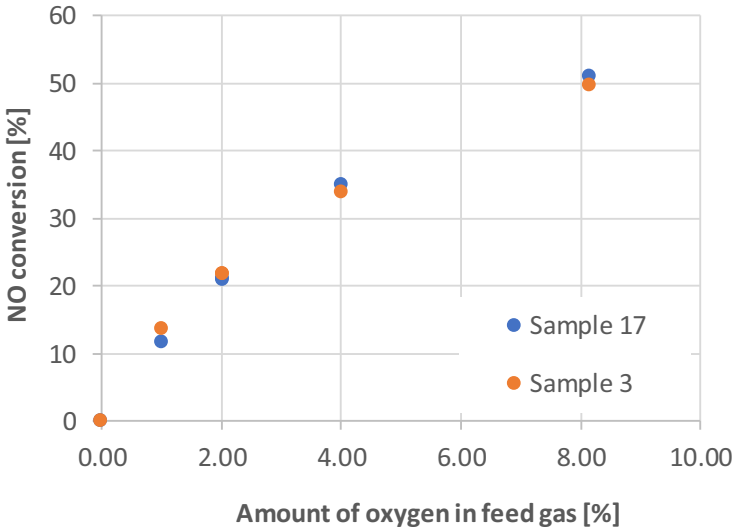

Fig. 6. Conversion of NO to NO_2 at 300 °C as a function of oxygen fraction present in the gas on two different samples of Pt-impregnated anodized cubic iso-reticular foams.

acquisition, Conceptualization, Investigation, Data curation, Writing - original draft. **Martin Fleissner Sunding:** Funding acquisition, Conceptualization, Investigation, Data curation, Writing - original draft. **Kari Anne Andreassen:** Funding acquisition, Conceptualization, Investigation, Data curation, Writing - original draft. **Jasmina Hafizovic Cavka:** Funding acquisition, Conceptualization, Investigation, Data curation, Writing - original draft. **Carlos A. Grande:** Funding acquisition, Conceptualization, Investigation, Data curation, Writing - original draft.

Acknowledgment

This work has received funding from the *European Union's Horizon 2020 research and innovation program* under grant agreement No 680414. The project belongs to the SPIRE program and information can be found in www.printcr3dit.eu.

Data availability

The raw/processed data required to reproduce these findings cannot be shared at this time.

Appendix A. Supplementary data

Supplementary data to this article can be found online at https://doi.org/10.1016/j.matdes.2019.108377.

References

[1] I. Fechete, Y. Wang, J.C. Védrine, The past, present and future of heterogeneous catalysis, Catal. Today 189 (2012) 2–27.
[2] K.P. de Jong (Ed.), Synthesis of Solid Catalysts, Wiley-VCH, Weinheim, Germany 2009, pp. 1–401.
[3] C.A. Grande, J-L Dubois, J.P.C. Camblor, Ø. Vistad, T. Didriksen, R. Blom, A.I. Spjelkavik, D. Akporiaye. Additive Manufacturing: Haute Couture for Chemical Industries, DOI: 10.13140/RG.2.1.1356.5520.
[4] A.S. Díaz-Marta, C.R. Tubío, C. Carbajales, C. Fernández, L. Escalante, E. Sotelo, F. Guitián, V.L. Barrio, A. Gil, A. Coelho, 3D printing in catalysis: combining 3D heterogeneous copper and palladium catalysts for multicatalytic multicomponent reactions, ACS Catal. 8 (2018) 392–404.
[5] C.R. Tubío, A. Rama, M. Gómez, F. del Río, F. Guitián, A. Gil, An efficient and recyclable 3D printed α-Al_2O_3 catalyst for the multicomponent assembly of bioactive heterocycles, Appl. Catal. A Gen. 530 (2017) 203–210.
[6] C. Parra-Cabrera, C. Achille, S. Kuhn, R. Ameloot, 3D printing in chemical engineering and catalytic technology: structured catalysts, mixers and reactors, Chem. Soc. Rev. 47 (2018) 209–230.
[7] X. Zhou, C.-J. Liu, Three-dimensional printing for catalytic applications: current status and perspectives, Adv. Funct. Mater. 27 (2017), 1701134.
[8] J.S. Manzano, Z.B. Weinstein, A.D. Sadow, I.I. Slowing, Direct 3D printing of catalytically active structures, ACS Catal. 7 (2017) 7567–7577.
[9] M. Konarova, W. Aslam, L. Ge, Q. Ma, F. Tang, V. Rudolph, J.N. Beltramini, Enabling process intensification by 3D printing of catalytic structures, ChemCatChem 9 (2017) 4132–4138.
[10] O.A. Alimi, N. Bingwa, R. Meijboom, Homemade 3-D printed flow reactors for heterogeneous catalysis, Chem. Eng. Res. Des. 150 (2019) 116–129.
[11] C.-Y. Lee, A.C. Taylor, A. Nattestad, S. Beirne, G.G. Wallace, 3D printing for electrocatalytic applications, Joule 3 (2019) 1835–1849.
[12] X. Li, W. Li, F. Rezaei, A. Rownaghi, Catalytic cracking of n-hexane for producing light olefins on 3D-printed monoliths of MFI and FAU zeolites, Chem. Eng. J. 333 (2018) 45–553.
[13] L. Martínez-Latorre, P. Ruiz-Cebollada, A. Monzón, E. García-Bordejé, Preparation of stainless steel microreactors coated with carbon nanofiber layer: impact of hydrocarbon and temperature, Catal. Today 147 (2009) S87–S93.
[14] S.A. Schmidt, N. Kumar, B. Zhang, K. Eränen, D.Y. Murzin, T. Salmi, Preparation and characterization of alumina-based microreactors for application in methyl chloride synthesis, Ind. Eng. Chem. Res. 51 (2012) 4545–4555.
[15] V. Meille, Review on methods to deposit catalysts on structured surfaces, Appl. Catal. A 315 (2006) 1–17.
[16] M.J. Ledoux, C. Pham-Huu, C. Silicon Carbide, A novel catalyst support for heterogeneous catalysis, CATTECH 5 (2001) 226–246.
[17] X. Fan, X. Ou, F. Xing, G.A. Turley, P. Denissenko, M.A. Williams, N. Batail, C. Pham, A.A. Lapkin, Microtomography-based numerical simulations of heat transfer and fluid flow through β-SiC open-cell foams for catalysis, Catal. Today 278 (2016) 350–360.
[18] D. Wu, H. Zhang, Mechanical stability of monolithic catalysts: scattering of washcoat adhesion and failure mechanism of active material, Ind. Eng. Chem. Res. 52 (2013) 14713–14721.
[19] M.A. Leon, R. Tschentscher, T.A. Nijhuis, J. van der Schaaf, J.C. Schouten, Rotating foam stirrer reactor: effect of catalyst coating characteristics on reactor performance, Ind. Eng. Chem. Res. 50 (2011) 3184–3193.
[20] M. Frey, T. Romero, A.-C. Roger, D. Edouard, Open cell foam catalysts for CO_2 methanation: presentation of coating procedures and *in situ* exothermicity reaction study by infrared thermography, Catal. Today 273 (2016) 83–90.
[21] L. Giani, C. Cristiani, G. Groppi, E. Tronconi, Washcoating method for Pd/γ-Al2O3 deposition on metallic foams, Appl. Catal. B Environ. 62 (2006) 121–131.
[22] S. Lim, R.A. Buswell, P.J. Valentine, D. Piker, S.A. Austin, X. De Kestelier, Modelling curved-layered printing paths for fabricating large-scale construction components, Addit. Manuf. 12 (2016) 216–230.
[23] I. Krimi, Z. Lafhaj, L. Ducoulombier, Prospective study on the integration of additive manufacturing to building industry—case of a French construction company, Addit. Manuf. 16 (2017) 107–114.
[24] V. Navrotsky, A. Graichen, H. Brodin, Industrialisation of 3D printing (additive manufacturing) for gas turbine components repair and manufacturing, VGB Powertech 12 (2015) 48–52.
[25] S. Limmahakhun, A. Oloyede, K. Sitthiseripratip, Y. Xiao, C. Yan, 3D-printed cellular structures for bone biomimetic implants, Addit. Manuf. 15 (2017) 93–101.
[26] A.M.M. Jani, D. Losic, N.H. Voelcker, Nanoporous anodic aluminium oxide: advances in surface engineering and emerging applications, Prog. Mater. Sci. 58 (2013) 636–704.
[27] C.A. Grande, K.A. Andreassen, J.H. Cavka, D. Waller, O.-A. Lorentsen, H. Øien, H.-J. Zander, S. Poulston, S. García, D. Modeshia, Process intensification in nitric acid plants by catalytic oxidation of nitric oxide, Ind. Eng. Chem. Res. 57 (2018) 10180–10186.
[28] L. Fratalocchi, C.G. Visconti, G. Groppi, L. Lietti, E. Tronconi, Intensifying heat transfer in Fischer-Tropsch tubular reactors through the adoption of conductive packed foams, Chem. Eng. J. 349 (2018) 829–837.

[29] S. Razza, T. Heidig, E. Bianchi, G. Groppi, W. Schwieger, E. Tronconi, H. Freund, Heat transfer performance of structured catalytic reactors packed with metal foam supports: influence of wall coupling, Catal. Today 273 (2016) 187–195.
[30] C. Busse, H. Freund, W. Schwieger, Intensification of heat transfer in catalytic reactors by additively manufactured periodic open cellular structures (POCS), Chem. Eng. Process. 124 (2018) 199–214.
[31] M. Klumpp, A. Inayat, J. Schwerdtfeger, C. Körner, R.F. Singer, H. Freund, W. Schwieger, Periodic open cellular structures with ideal cubic cell geometry: effect of porosity and cell orientation on pressure drop behavior, Chem. Eng. J. 242 (2014) 364–378.
[32] N.F. Bastos Rebelo, K.A. Andreassen, L.I. Suarez Ríos, J.C. Piquero Camblor, H.-J. Zander, C.A. Grande, Pressure drop and heat transfer properties of cubic isoreticular foams, Chem. Eng. Process. 127 (2018) 36–42.
[33] S. Nawada, S. Dimartino, C. Fee, Dispersion behavior of 3D-printed columns with homogeneous microstructures comprising differing element shapes, Chem. Eng. Sci. 164 (2017) 90–98.
[34] V.H. Henley, Anodic Oxidation of Aluminium and Its Alloys, Pergamon Press, Oxford, 1982.
[35] J.M. Torrescano-Alvarez, M. Curioni, H. Habazaki, T. Hashimoto, P. Skeldon, X. Zhou, Incorporation of alloying elements into porous anodic films on aluminium alloys: the role of cell diameter, Electrochim. Acta 296 (2019) 783–789.
[36] M.M. Abbas, Electrochemical Self-assembly of Nanoporous Alumina, 3, AMPC, 2013 244–248.
[37] P.C. Stair, C. Marshall, G. Xiong, H. Feng, M.J. Pellin, J.W. Elam, L. Curtiss, L. Iton, H. Kung, M. Kung, H.-H. Wang, Novel, uniform nanostructured catalytic membranes, Top. Catal. 39 (2006) 181–186.
[38] B.R. Tzaneva, A.I. Naydenov, S.Z. Todorova, V.H. Videkov, V.S. Milusheva, P.K. Stefanov, Cobalt electrodeposition in nanoporous anodic aluminium oxide for application as catalyst for methane combustion, Electrochim. Acta 191 (2016) 192–199.
[39] F.J. Méndez, O. Sanz, M. Montes, J. Guerrac, C. Olivera-Fuentes, S. Curbelo, J.L. Brito, Selective hydrogenation of 1,3-butadiene in the presence of 1-butene under liquid phase conditions using structured catalyst, Catal. Today 289 (2017)(151-16).
[40] T. Tomita, A. Uesugi, Y. Hotta, Y. Hatanaka, Catalyst body which uses an anodized layer, Eur. Pat. Appl. 1994982A1 (March 30, 2007).
[41] M. Moskovits. Heterogeneous Catalyst and Process for its Manufacture, U.S. Patent 4,472,533, December 15, 1982.
[42] L.A. Coady. Catalyst Including Anodized Aluminium Substrate and Method of Manufacture, Eur. Pat. Appl. EP0281364 A2, March 4, 1987.
[43] A.L. Friedman, D. Brittain, L. Menon, Roles of pH and acid type in the anodic growth of porous alumina, J. Chem. Phys. 127 (2007), 154717.
[44] S.Z. Chu, K. Wada, S. Inoue, M. Isogai, Y. Katsuta, A. Yasumori, Large-scale fabrication of ordered nanoporous alumina films with arbitrary pore intervals by critical-potential anodization, J. Electrochem. Soc. 153 (2006) B384–B391.
[45] S. Ono, M. Saito, H. Asoh, Self-ordering of anodic porous alumina formed in organic acid electrolytes, Electrochim. Acta 51 (2005) 827–833.
[46] W. Lee, J.C. Kim, Highly ordered porous alumina with tailor-made pore structures fabricated by pulse anodization, Nanotechnology 21 (2010), 485304.
[47] L. Yi, L. Zhiyuan, C. Shuoshuo, H. Xing, H. Xinhua, Novel AAO films and hollow nanostructures fabricated by ultra-high voltage hard anodization, Chem. Commun. 46 (2010) 309–311.
[48] F. Zhang, X. Liu, C. Pan, J. Zhu, Nano-porous anodic aluminium oxide membranes with 6–19 nm pore diameters formed by a low-potential anodizing process, Nanotechnology 18 (2007), 345302.
[49] K. Lee, Y. Tang, M. Ouyang, Self-ordered, controlled structure nanoporous membranes using constant current anodization, Nano Lett. 8 (2008) 4624–4629.
[50] W. Lee, J.C. Kim, U. Gösele, Spontaneous current oscillations during hard anodization of aluminum under potentiostatic conditions, Adv. Funct. Mater. 20 (2010) 21–27.
[51] G.D. Sulka, W.J. Stepniowski, Structural features of self-organized nanopore arrays formed by anodization of aluminum in oxalic acid at relatively high temperatures, Electrochim. Acta 54 (2009) 3683–3691.
[52] J. Choi, R.B. Wehrspohn, U. Gösele, Mechanism of guided self-organization producing quasi-monodomain porous alumina, Electrochim. Acta 50 (2005) 2591–2595.
[53] H. Masuda, F. Hasegwa, S. Ono, Self-ordering of cell arrangement of anodic porous alumina formed in sulfuric acid solution, J. Electrochem. Soc. 144 (1997) L127–L130.
[54] I. Vrublevsky, V. Parkoun, J. Schreckenbach, Analysis of porous oxide film growth on aluminum in phosphoric acid using re-anodizing technique, Appl. Surf. Sci. 242 (2005) 333–338.
[55] J.J. Schneider, J. Engstler, K.P. Budna, C. Teichert, S. Franzka, Freestanding, highly flexible, large area, nanoporous alumina membranes with complete through-hole pore morphology, Eur. J. Inorg. Chem. (2005) 2352–2359.
[56] A.C. Crossland, G.E. Thompson, C.J.E. Smith, H. Habazaki, K. Shimizu, P. Skeldon, Formation of manganese-rich layers during anodizing of Al-Mn alloys, Corros. Sci. 41 (1999) 2053–2069.
[57] H. Habazaki, K. Shimizu, P. Skeldon, G.E. Thompson, G.C. Wood, The co-enrichment of alloying elements in the substrate by anodic oxidation of Al-Cu-W alloys, Corros. Sci. 39 (1997) 339–354.
[58] H. Habazaki, K. Shimizu, P. Skeldon, G.E. Thompson, G.C. Wood, X. Zhou, Nanoscale enrichments of substrate elements in the growth of thin oxide films, Corros. Sci. 39 (1997) 731–737.
[59] K. Shimizu, G.M. Brown, K. Kobayashi, P. Skeldon, G.E. Thompson, G.C. Wood, Ultramicrotomy—a route towards the enhanced understanding of the corrosion and filming behaviour of aluminium and its alloys, Corros. Sci. 40 (1998) 1049–1072.
[60] K. Shimizu, G.M. Brown, H. Habazaki, K. Kobayashi, P. Skeldon, G.E. Thompson, G.C. Wood, Selective oxidation of aluminium and interfacial enrichment of iron during anodic oxide growth on an Al_6Fe phase, Corros. Sci. 42 (2000) 831–840.
[61] I. Tsangaraki-Kaplanoglou, S. Theohari, T. Dimogerontakis, Y.M. Wang, H.H. Kuo, S. Kia, Effect of alloy types on the anodizing process of aluminum, Surf. Coat. Technol. 200 (2006) 2634–2641.
[62] X. Zhou, G.E. Thompson, P. Skeldon, G.C. Wood, K. Shimizu, H. Habazaki, Film formation and detachment during anodizing of Al-Mg alloys, Corros. Sci. 41 (1999) 1599–1613.
[63] J.B. Franklin, Jr. N. W. Vallance. Process for Producing Oxide Coatings on High Silicon Aluminum alloy, U.S. Patent. 3,020,219A, January 12, 1959.
[64] G. Mul, J.A. Moulijn, Preparation of supported metal catalyst, in: J.A. Anderson, M.F. Garcia (Eds.), Supported Metals in Catalysis, Catalytic Science Series, vol 5, Imperial Collage Press 2005, pp. 1–32.
[65] E. Joubert, X. Courtois, P. Marecot, D. Duprez, NO reduction by hydrocarbons and oxygenated compounds in O_2 excess over a Pt/Al_2O_3 catalyst - a comparative study of the efficiency of different reducers (hydrocarbons and oxygenated compounds), Appl. Catal. B Environ. 64 (2006) 103–110.
[66] J.R.A. Sietsma, J.D. Meeldijk, J.P. Breejen, M. Versluijs-Helder, J. Dillen, P.E. de Jongh, K.P. de Jong, The preparation of supported NiO and Co_3O_4 nanoparticles by the nitric oxide controlled thermal decomposition of nitrates, Angew. Chem. Int. Ed. 46 (2007) 4547–4549.